Limited Diffraction Array Beams

Jian-yu Lu

Ultrasound Research Laboratory, Department of Physiology and Biophysics, Mayo Clinic and Foundation, Rochester, MN 55905

ABSTRACT: Limited diffraction beams have a large depth of field and could have many applications. In this article, new limited diffraction beams are developed. They are composed of multiple parallel beams and are thus called array beams. A broadband synthetic array experiment is used to produce these beams of a finite aperture, and results are in excellent agreement with theory over a large depth of field. In addition, potential applications of the new beams to real-time volumetric imaging and measurement of transverse velocity of blood flow are described. © 1997 John Wiley & Sons, Inc. Int J Imaging Syst Technol, **8,** 126–136, 1997

Keywords: X waves; Bessel beams; limited diffraction beams; real-time 2D and 3D imaging; transverse doppler effects

I. INTRODUCTION

Limited diffraction beams have an infinite depth of field if they are produced with an infinite aperture [1–3]. Even if produced with a finite aperture, they have a large depth of field [1]. Because of this, limited diffraction beams could have applications in medical imaging [3–26], tissue characterization [27], nondestructive evaluation of materials (NDE) [28–30], Doppler velocity estimation [31], and other areas such as electromagnetics [32,33] and optics [34]. In the following, a brief background on the development of beams of a large depth of field is given.

Conventional focused beams are widely used in various areas but they have a short depth of field [35]. They have a small beamwidth or high lateral resolution in imaging around their focal region. Away from the focus, beams diverge or spread very quickly, especially for a smaller *f*-number (focal length divided by aperture diameter). When these beams are applied to pulse-echo medical imaging, multiple transmissions of beams focused at different depths are needed to increase an effective depth of field. Because transmission of a beam must wait until all echoes of previous one return and the propagation speed of sound in biologic soft tissues is limited, multiple transmissions reduce image frame rate greatly. A low frame rate blurs images of moving objects such as the heart.

To overcome the problem of the small depth of field of conventional focused beams, various methods have been developed. For example, McLeod [36] invented an optical device in 1954 that has a large depth of field and is called Axicon. This device was implemented in acoustics by Burckhardt et al. in 1973 [37] and was further studied by many investigators [38–41]. Unlike limited diffraction beams, beams produced by an Axicon change with propagation distance even if they are produced with an infinite aperture. Because of their high side lobes and complex beam patterns near the cone surface, these devices are not currently used in clinics. Ring antenna [42] or transducer [43,44] is another type of device that increases the depth of field. However, the depth of field is increased only in the far field of the rings [45,46] where beams diffract significantly. Near the surfaces of the rings, beams do not even have a central peak. In addition, ring devices have a low energy efficiency because they must be thin. Dynamic focusing [47] is another method to increase the depth of field, in which the focal length of a receiver increases with the distance so that echoes are always in focus. Combined with a dynamic aperture technique [48], dynamic focusing may produce a constant *f*-number and thus have a constant lateral beamwidth or resolution in imaging over the depth of interest. However, this method can be applied only in reception [47]. Other methods that increase the depth of field are reviewed in Reference [3].

Recently, new beams that have a large depth of field were developed. These beams are called localized waves and can propagate to a large distance with only local deformation. Localized waves were first discovered by Brittingham in 1983 and were termed ''focus wave modes'' [49]. They were further studied by Ziolkowski et al. [50,51] and many other investigators [52–59]. Independent of Brittingham and Ziolkowski's work, in 1987, Durnin performed the first experimental study of a limited diffraction beam [1]. Unlike localized waves, in theory, limited diffraction beams can propagate to an infinite distance without changing their sharply focused beam shapes. Durnin termed the new beams ''nondiffracting beams'' [1] or ''diffraction-free beams'' [2]. Because Durnin's terminologies are controversial in scientific communities, a new term, ''limited diffraction beams,'' has been used on the basis that all practical beams will diffract eventually [3]. Durnin's beams (also called Bessel beams because their lateral beam profiles are a Bessel function) have been further studied in both optics [34,60,61] and acoustics [29,30].

More recently, a new type of limited diffraction beams was discovered. They were obtained by directly solving the wave equation. These beams are called X waves because they have an X-like shape in a plane along the beam axis [15–18]. X waves also have a large depth of field but are different from Bessel beams because they are nondispersive (speed of waves are not a function of frequency) in an isotropic/homogeneous medium. The nondispersive property of X waves may be useful for image restoration where the point spread function of an imaging system is depth independent [4,23].

In this article, another new type of limited diffraction beams

Contract grant sponsor: National Institutes of Health; *Contract grant number:* CA 54212; *Contract grant number:* CA 43920

 CCC 0899–9457/97/010126-11

is developed. These beams are called array beams because they are composed of multiple parallel sub-beams that form an array pattern in a plane perpendicular to the beam axis. A broadband synthetic array experiment was developed to produce these beams of a finite aperture, and results are in excellent agreement with those of theoretical beams over a large depth of field. In addition, potential applications of these beams to real-time volumetric imaging [62–67] and the measurement of transverse velocity of blood flow [31,68,69] are described.

II. THEORY

In this section, array beams will be derived from a general limited diffraction solution of an N-dimensional wave equation.

A. Limited Diffraction Solutions. The N-dimensional isotropic/homogeneous scalar wave equation is given by [70]

$$\left[\sum_{j=1}^{N}\frac{\partial^2}{\partial x_j^2}-\frac{1}{c^2}\frac{\partial^2}{\partial t^2}\right]\Phi=0, \tag{1}$$

where x_j, ($j = 1, 2, \ldots, N$), represent rectangular coordinates in an N-dimensional space, t is time, N is an integer that is >0, c is a constant, and $\Phi = \Phi(x_1, x_2, \ldots, x_N; t)$ is an N-dimensional wave field.

One family of solutions of Equation (1) is given by [4]

$$\Phi(x_1, x_2, \ldots, x_N; t) = f(s), \tag{2}$$

where

$$s=\sum_{j=1}^{N-1}D_jx_j+D_N(x_N-c_1t),\quad (N\geq 1), \tag{3}$$

and where D_j are complex coefficients that are independent of the spatial and time variables (x_j ($j = 1, 2, \ldots, N$) and t), $f(s)$ is any well-behaved complex function of s, and

$$c_1=c\sqrt{1+\sum_{j=1}^{N-1}D_j^2/D_N^2},\quad (N\geq 1). \tag{4}$$

If c_1 is real, Equation (2) and its linear combinations represent limited diffraction solutions of Equation (1).

B. Bessel Array Beams. If $N = 3$, Equation (1) is a three-dimensional wave equation. Assume that $x_1 = x$, $x_2 = y$, $x_3 = z$, $D_1 = -i\alpha \cos\theta$, $D_2 = -i\alpha \sin\theta$, and $D_3 = i\beta$, where α is a constant, θ is a free parameter, and $\beta = \sqrt{k^2 - \alpha^2} > 0$, where $k = \omega/c$ is the wave number and ω is the angular frequency, from Equation (3) one obtains

$$s = -i\alpha(x\cos\theta + y\sin\theta) + i\beta(z - c_1t), \tag{5}$$

where

$$c_1 = c\sqrt{1+\alpha^2/\beta^2} = \omega/\beta. \tag{6}$$

Let $f(s) = e^s$ and integrate $f(s)$ over θ, one obtains the nth-order Bessel beams [15,1]

$$\Phi_{J_n}(s)=\frac{1}{2\pi}\int_{-\pi}^{\pi}A(\theta)f(s)\,d\theta = J_n(\alpha r)e^{i(\beta z-\omega t+n\phi)}, \tag{7}$$

where $A(\theta) = i^n e^{in\theta}$, n is an integer that is ≥ 0, the subscript ''J_n'' means ''nth-order Bessel beams,'' $J_n(\cdot)$ is the nth-order Bessel function of the first kind [71], and $r = \sqrt{x^2 + y^2}$ and $\phi = \tan^{-1}(y/x)$ are variables in the polar coordinates.

Taking the mth-derivative of Equation (7) in terms of both variables x and y, one obtains the Bessel array beams

$$\Phi^{A_m}_{J_n^m}(r, \phi, z - c_1t) = \frac{\partial^{2m}}{\partial x^m\partial y^m}\Phi_{J_n}(r, \phi, z - c_1t), \tag{8}$$

where the superscript ''A_m'' means ''mth-derivative array beams,'' and m is an even integer that is >0. It is noticed that $\Phi^{A_m}_{J_n^m}$ in Equation (8) is also a solution to the wave equation (1) [this can be verified by directly inserting Eq. (8) into (1), exchanging the order of derivatives, and then using the fact that Φ_{J_n} is a solution to (1)]. For simplicity, in the following we assume that $n = 0$ in Equation (8), where Φ_{J_0} is called the *zero*th-order Bessel beam. To see the trend of beam patterns of (8) with m, two examples are given for $m = 4$ and 10.

Transverse patterns of $|\Phi^{A_m}_{J_0^m}(r, \phi, z - c_1t)|$, ($r \leq D/2$), at $z = c_1t$ for $m = 4$ and 10 are shown in the panels (a) and (b) respectively, of Figure 1, where $D = 50$ mm is the diameter of the aperture. It is seen that as m increases, the number of beam grids increases, too. Theoretically, if $D \to \infty$, the field patterns shown in Figure 1(a) and 1(b) will stay forever as the beams propagate to an infinite distance (nondiffracting).

C. Grid Array Beams. Choosing different parameters, one obtains from Equation (2) a limited diffraction beam that has a larger grid area than the Bessel array beams. Let $l = 3$, $x_1 = x$, $x_2 = y$, $x_3 = z$, $D_1 = \pm ik_x$, $D_2 = \pm ik_y$, and $D_3 = ik_z$, where k_x and k_y are the x and y components of the vector wave number $\mathbf{k} = (\pm k_x, \pm k_y, k_z)$, respectively, where ''$\pm$'' means that either the plus or minus sign can be selected, and where $k_z = \sqrt{k^2 - k_x^2 - k_y^2} > 0$ and $k = |\mathbf{k}| = \omega/c$, from Equation (3), one obtains four different s:

$$\begin{cases} s_1 = +ik_xx + ik_yy + ik_z(z - c_1t),\\ s_2 = -ik_xx + ik_yy + ik_z(z - c_1t),\\ s_3 = +ik_xx - ik_yy + ik_z(z - c_1t),\\ s_4 = -ik_xx - ik_yy + ik_z(z - c_1t), \end{cases} \tag{9}$$

where

$$c_1 = c\sqrt{1+(k_x^2+k_y^2)/k_z^2} = \omega/k_z. \tag{10}$$

Substituting Equation (9) into (2) and using the following linear combination, $\{[f(s_1) + f(s_2)]/2 + [f(s_3) + f(s_4)]/2\}/2$, where $f(s_j) = e^{s_j}$ ($j = 1, 2, 3, 4$), one obtains grid array beams:

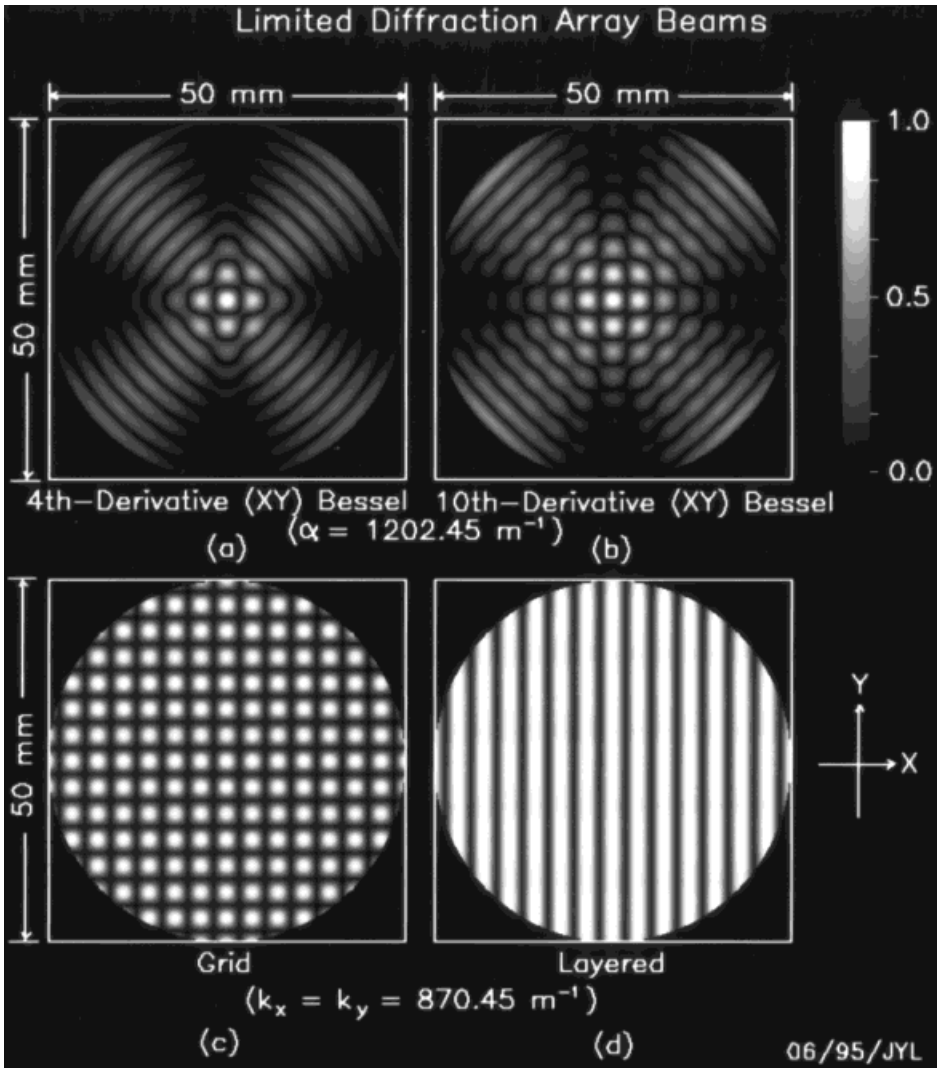

Figure 1. Limited diffraction array beams obtained from the theoretical solutions of the wave Equation (1): (a) Fourth-derivative Bessel array beam; (b) 10th-derivative Bessel array beam, (c) grid array beam, and (d) layered array beam. These beams are shown in a diameter of 50 mm. The parameter of the beams ($\alpha = 1202.45$ m^{-1}, and $k_x = k_y = 870.45$ m^{-1}) are chosen so that their grid sizes are comparable. The images shown in the panels are the peak of the absolute values of the beams at every point (x, y) in a plane perpendicular to the propagation axis of the beams (e.g., at $z = c_1t$) and are displayed from 0 to 1 in 256 gray-scales.

$$\Phi_G(x, y, z - c_1t) = (\cos k_x x)(\cos k_y y)e^{ik_z(z-c_1t)}, \qquad (11)$$

where the subscript ''G'' means ''grid.''

A transverse pattern of a grid array beam $|\Phi_G(x, y, z - c_1t)|$ in Equation (11) at $z = c_1t$ is shown in Figure 1(c) with the parameter $k_x = k_y = 870.45$ m^{-1} ($D = 50$ mm).

D. Layered Array Beams. Solving a two-dimensional wave equation [$N = 2$ in Eq. (1)], one obtains layered array beams. Let $x_1 = x$, $x_2 = z$, $D_1 = \pm ik_x$, and $D_2 = ik_z$, where k_x is the x component of the vector wave number $\mathbf{k} = (\pm k_x, k_z)$, where $k_z = \sqrt{k^2 - k_x^2} > 0$ and $k = |\mathbf{k}| = \omega/c$, from Equation (3), one obtains two different s:

$$\begin{cases} s_1 = +ik_x x + ik_z(z - c_1t), \\ s_2 = -ik_x x + ik_z(z - c_1t), \end{cases} \qquad (12)$$

where

$$c_1 = c\sqrt{1 + k_x^2/k_z^2} = \omega/k_z. \qquad (13)$$

Substituting Equation (12) into (2) and using the following linear combination, $[f(s_1) + f(s_2)]/2$, where $f(s_j) = e^{s_j}$ ($j = 1, 2$), one obtains layered array beams:

$$\Phi_L(x, z - c_1t) = (\cos k_x x)e^{ik_z(z-c_1t)}, \qquad (14)$$

where the subscript ''L'' means ''layered.'' It is noted that the layered array beams in Equation (14) are independent of y.

A transverse pattern of a layered array beam $|\Phi_L(x, z - c_1t)|$ in Equation (14) at $z = c_1t$ is shown in panel (d) of Figure 1 with the parameter $k_x = 870.45$ m^{-1} ($D = 50$ mm). The parallel structure of the beam layers in Figure 1(d) will remain unchanged for all t if the beam is produced with an infinite aperture $D \to \infty$. With layered array beams, the transverse velocity of blood flow can be measured without using a wedge stand.

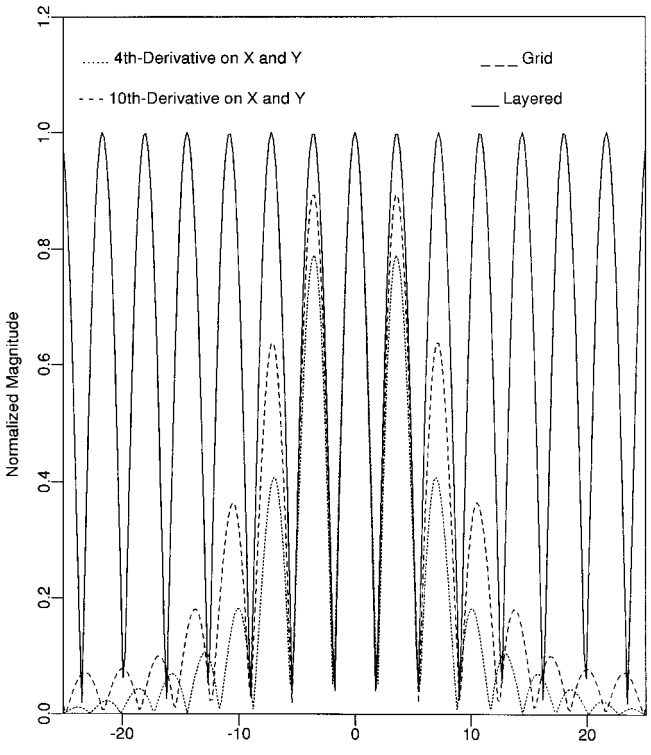

Figure 2. Line plots of the array beams in Figure 1 through the x axis at $y = 0$. The fourth- and 10th-derivative Bessel array beams are shown with dotted and dashed lines, respectively. The grid array beam and the layered array beam are shown with long dashed and full lines. Because the parameter k_x is the same for both grid and layered array beams, their line plots are virtually overlapped. The vertical axis of the plots is normalized magnitude and the lateral axis is from −25 to 25 mm.

E. Line Plots of Array Beams. To show the details of the patterns of the theoretical array beams in Figure 1, line plots through the x axis (at $y = 0$) are given in Figure 2. These plots show that as the order of derivative increases, Bessel array beams approach a grid array beam (see the changes of the intergrid distances and the magnitude of the grids of the Bessel array beams).

III. EXPERIMENT

In this section, a broadband synthetic array experiment was used to produce limited diffraction array beams. Results were compared to those of the theoretical beams.

Similar to a plane wave, a theoretical limited diffraction array beam given by Equation (8), (11), or (14) cannot be produced in practice because it requires an infinite aperture. However, it can be approximately produced over a large depth of field with a two-dimensional array transducer of a finite aperture and a finite number of elements. The larger the number is of elements of an array, the better the aperture weighting functions or beams are approximated. However, a two-dimensional array of a large number of elements is difficult to make. Instead of using such an array, a synthetic array experiment [72,73] can be used to produce the array beams.

In the experiment, a small transducer of a diameter of about 1 mm was used. The transducer was broadband (its −6-dB relative bandwidth was about 80%) and its central frequency was 2.5 MHz. Because short pulses are desired for imaging, instead of a continuous-wave (CW) waveform required by Equations (8), (11), and (14), a broadband pulse with a time duration of about 1.5 cycles was used to drive the transducer. The transducer was immersed in water and scanned in a raster format firing sequentially on the positions where the elements of a two-dimensional array would exist. The distance between firings was 0.2 mm and the excitation pulse was weighted with the function, Equation (8), (11), or (14), evaluated at the distance $z = c_1 t = 0$, as the transducer moved from one position to another. A 0.5-mm diameter hydrophone (NTR System) was placed at a fix point some distance away from the scanning plane and the acoustic waves measured with the hydrophone were coherently summed to give the response of that point. The summation was done for those transducer positions that were within a 50-mm diameter which defined the aperture of the synthetic array. To obtain acoustic responses along a line, the position of the hydrophone was changed relative to the scanning aperture in a step of 0.2 mm.

Experiment results of the array beams and their comparison with those of the CW theoretical beams are shown in Figure 3. It is seen that the broadband or pulse wave (PW) beams do not change the intergrid distances or the parallel structures of the CW beams. This means that PW array beams can also be used for the real-time volumetric imaging and the measurement of transverse velocity of blood flow. Because the experimental beams have a finite aperture, they have a finite depth of field and are only approximations of the theoretical beams. Within the depth of field (see panels in the left column for $z = 100$ mm), the experiment is in an excellent agreement with the theory. Near the boundary of the depth of field ($z = 216$ mm), the experimental beams start to spread.

Because an array beam of a phase velocity, c_1, where $c_1 > c$, can be represented with a linear superposition of Bessel beams of the same phase velocity but of different orders [74,75], it has the same depth of field as the Bessel beams. The depth of field of a Bessel beam is given by [75,74] (derived from [1,15])

$$Z_{\max} = a \frac{1}{\sqrt{\left(\frac{c_1}{c}\right)^2 - 1}}, \tag{15}$$

where a is the radius of the aperture. With the parameters given in Figure 1 and the experiment above, the phase velocities of the Bessel array beams, grid array beams, and layered array beams are given by

$$c_1 = \frac{\omega}{\beta} = \frac{\omega}{\sqrt{k^2 - \alpha^2}} = 1509.99 \text{ m/s}, \tag{16}$$

$$c_1 = \frac{\omega}{k_z} = \frac{\omega}{\sqrt{k^2 - k_x^2 - k_y^2}} = 1510.47 \text{ m/s}, \tag{17}$$

and

$$c_1 = \frac{\omega}{k_z} = \frac{\omega}{\sqrt{k^2 - k_x^2}} = 1505.21 \text{ m/s}, \tag{18}$$

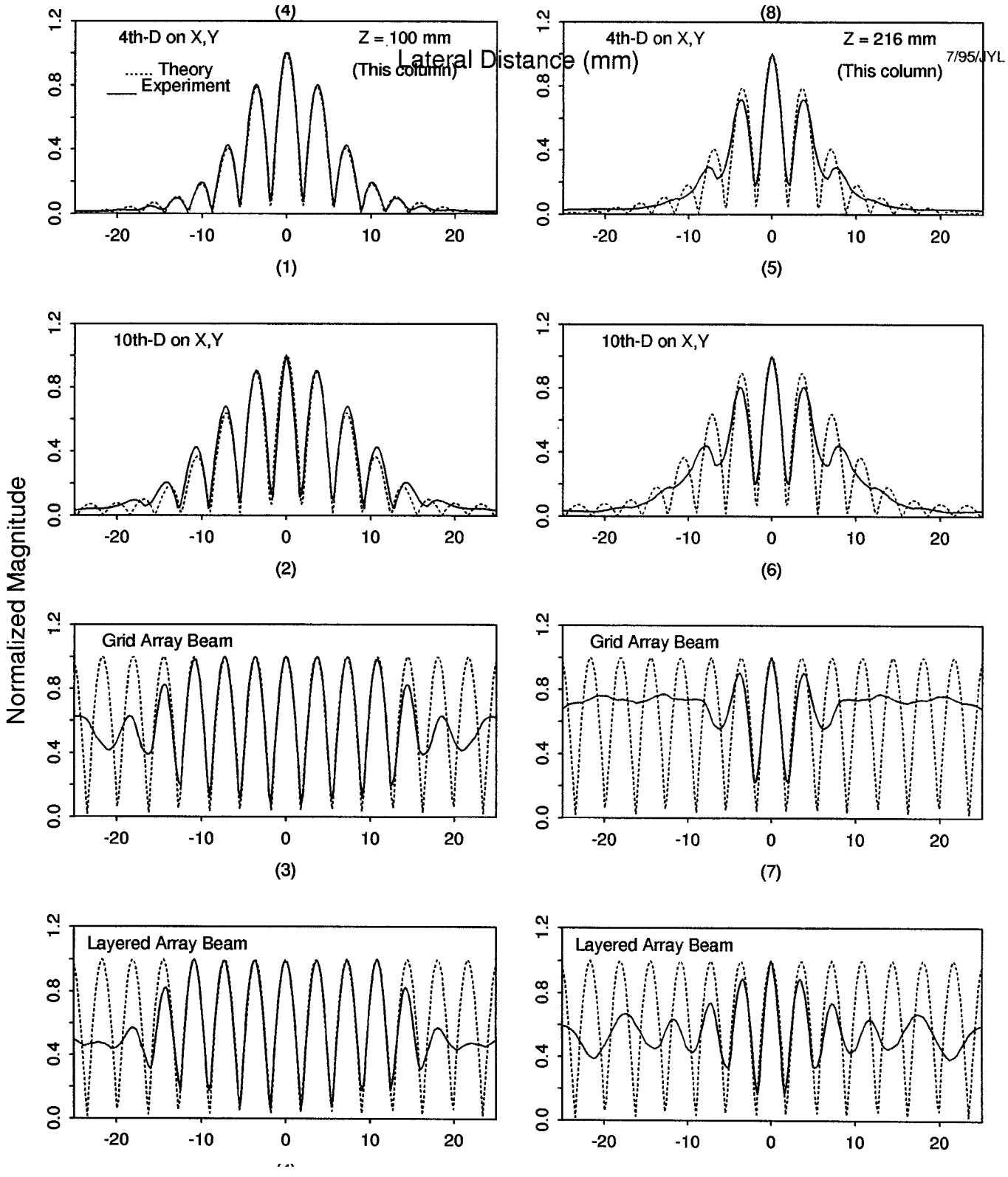

Figure 3. Line plots of limited diffraction array beams obtained with a broadband synthetic array experiment (full lines) at two axial distances, $z = 100$ mm (panels in the left column) and 216 mm (panels in the right column). The plots show the peaks of the magnitudes of the beams evaluated on the x axis (lateral distance) at $y = 0$. The panels in the rows from the top to bottom correspond to the fourth- and 10th-derivative Bessel array beams, the grid array beam, and the layered array beam, respectively. For comparison, plots from Figure 2 are added accordingly (dotted lines). The vertical and the lateral axes are the same as those in Figure 2. Notice that the experiment data were obtained from $x = 0$ to 25 mm and plots from $x = -25$ to 0 mm were mirrored accordingly because beams should be symmetric about the y axis.

respectively, resulting in depths of field of 216.28, 211.20, and 299.72 mm.

For broadband array beams, the depths of field calculated from Equation (15) are approximately true because the spectrum of the pulse used in the experiment was strongly peaked at the central frequency of 2.5 MHz. This was shown in many previous publications [3,4,7,8,15,16].

IV. POSSIBLE APPLICATIONS

Limited diffraction array beams have parallel beam structures as well as a large depth of field. Therefore, they have potential applications in real-time volumetric imaging and measurement of transverse velocity of blood flow.

A. Volumetric Imaging. Ultrasonic volumetric imaging can be viewed as a stack of two-dimensional B-mode images. Because the speed of sound in objects such as biologic soft tissues is finite, the image frame rate of conventional B-mode scanners is limited, especially when imaging a large region of interest. In volumetric imaging, the image frame rate will be further reduced by the number of B-mode images stacked. Therefore, it is necessary to apply parallel processing (beam forming) for received signals. The parallel beam forming requires a simultaneous acoustic illumination of an area in which multiple receive beams are formed [62,63] or a simultaneous transmission of multiple focused beams to cover the area. Because array beams such as grid array beams are composed of multiple parallel pencil beams (stay in focus over a large distance and each sub-beam has a high lateral resolution) (Fig. 4), they could be used to illuminate a larger area while improving lateral resolution over a large depth of field in real-time volumetric imaging.

A real-time volumetric imaging system with a grid array beam is described as follows. With a grid array beam, parallel pencil beams are transmitted simultaneously to illuminate an area of interest. Each pencil beam has its well-defined boarders and the thickness of the beam does not change from the surface of transducer to a predefined depth of interest (depth of field). In receive, transducer elements can be weighted using conventional techniques to form multiple receive beams (parallel beam forming) and to focus the beams dynamically with a dynamic aperture. Because transmit beams have a large depth of field, multiple transmissions to refocus the beams at different depths are not necessary. In addition, because all beams in a grid array beam are pencil-like, they have a better lateral definition of a resolution cell than a broad transmission beam [62] that fills up the gaps between the multiple beams of a grid array beam. A schematic of using a grid array beam in volumetric imaging is shown in Figure 4. Other array beams such as the Bessel array beams could also be used.

B. Measurement of Transverse Velocity of Blood Flow. Assuming that a layered array beam is given by Equation (14), and a point receiver is moving in the $x-z$ plane at a velocity v that makes an angle θ with the z axis, we can write the position of the receiver [31,68]

$$\begin{cases} x = x_0 + vt \sin\theta \\ z = z_0 + vt \cos\theta \end{cases} \tag{19}$$

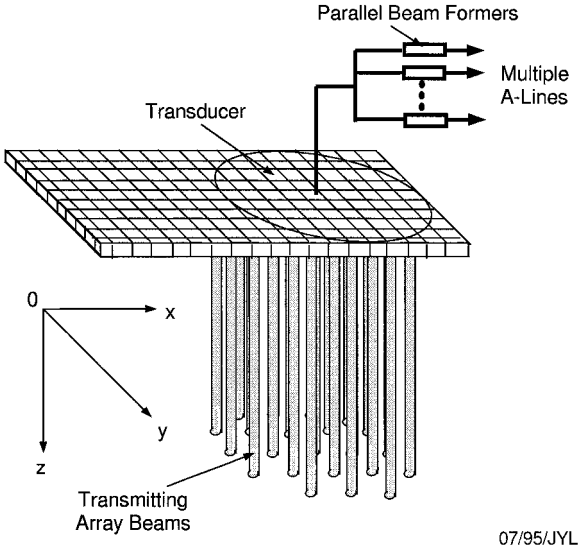

Figure 4. A schematic of a limited diffraction grid array beam for real-time volumetric imaging. A two-dimensional array transducer is driven with a short pulse (say, one and a half cycles) and weighted with (11) to produce an approximate grid array beam. Echoes returned from scattering materials will be picked up by the same transducer that forms multiple dynamically focused receive beams that follow the parallel transmission beams. The simultaneous formation of parallel receiving beams will increase image frame rate. Because grid array beams are limited diffraction beams, the lateral width of the grid of the transmission beam will remain constant over a large depth of field (Fig. 3). The transducer can be scanned electronically or mechanically in a raster format within a grid area in the $x-y$ plane to increase the density of A-lines in the cylindrical volume.

where (x_0, z_0) is the position of the receiver at $t = 0$. Substituting Equation (19) into (14) and ignoring the secondary Doppler effects (Doppler effects caused by frequency shift), we obtain [31]

$$\begin{aligned} g(\vec{r}_0, t) &= \cos[k_x(x_0 + vt \sin\theta)]e^{ik_z(z_0 + vt\cos\theta) - i\omega_0 t} \\ &= \cos\left[k_x v \sin\theta\left(t - \frac{-x_0}{v \sin\theta}\right)\right]e^{i(k_z v\cos\theta - \omega_0)t}e^{ik_z z_0} \end{aligned} \tag{20}$$

where ω_0 is the angular frequency of the received signal when $v = 0$ and $k_z = \sqrt{k_0^2 - k_x^2}$, where $k_0 = \omega_0/c$.

If we use the following definition of the Fourier transform

$$G(\omega) = \int_{-\infty}^{\infty} g(t)e^{i\omega t}\,dt \tag{21}$$

we have the Fourier transform pair

$$\cos\alpha t \leftrightarrow \pi[\delta(\omega + \alpha) + \delta(\omega - \alpha)]. \tag{22}$$

From Equations (20) and (21) and using the shift and modulation theorems of the Fourier transform, we obtain

$$\begin{aligned} G(\vec{r}_0, \omega) = \pi[&\delta(\omega' + k_x v \sin\theta) \\ &+ \delta(\omega' - k_x v \sin\theta)]e^{-i(x_0/v\sin\theta)\omega'}e^{ik_z z_0} \end{aligned} \tag{23}$$

where

$$\omega' = \omega - (\omega_0 - k_z v \cos\theta). \tag{24}$$

In Equations (23) and (24), we notice that $k_x v \sin\theta$ and $k_z v \cos\theta$ are frequency shifts caused by the transverse beam modulation of received signals and the Doppler effects, respectively.

From Equation (14) we obtain the pulsed-echo response of a layered array beam from a point scatterer

$$\Phi_{Lb}(x, z - c_1 t) = (\cos^2 k_x x) e^{2ik_z z - i\omega_0 t}, \tag{25}$$

where the subscript ''*b*'' means ''backscattered.'' Substituting Equation (19) into (25), one obtains a backscattered signal from a moving point scatter

$$g_b(\vec{r}_0, t) = \cos^2\left[k_x v \sin\theta\left(t - \frac{-x_0}{v \sin\theta}\right)\right] e^{i(2k_z v\cos\theta - \omega_0)t} e^{i2k_z z_0}. \tag{26}$$

With the Fourier transform, we obtain the spectrum

$$G_b(\vec{r}_0, \omega) = \pi\delta(\omega') e^{i2k_z z_0} + \frac{\pi}{2}[\delta(\omega' + 2k_x v \sin\theta) + \delta(\omega' - 2k_x v \sin\theta)] e^{-i(x_0/v\sin\theta)\omega'} e^{i2k_z z_0} \tag{27}$$

where

$$\omega' = \omega - (\omega_0 - 2k_z v \cos\theta). \tag{28}$$

We see that the spectrum of the pulsed-echo response of a layered array beam transducer is composed of three line spectra at

$$\omega = \omega_c, \tag{29}$$

$$\omega = \omega_c - 2k_x v \sin\theta, \tag{30}$$

and

$$\omega = \omega_c + 2k_x v \sin\theta, \tag{31}$$

respectively, where

$$\omega_c = \omega_0 - 2k_z v \cos\theta \tag{32}$$

is the new central frequency caused by the Doppler effects. From Equations (30) and (31), we see that the distance (bandwidth) between the two side-line spectra is given by

$$\omega_b = 4k_x v \sin\theta. \tag{33}$$

From Equations (32) and (33), we obtain both the velocity and its angle with respect to the *z* axis [31,68]

$$v = \frac{1}{2}\sqrt{\left(\frac{\omega_b}{2k_x}\right)^2 + \left(\frac{\omega_c - \omega_0}{k_z}\right)^2} \tag{34}$$

and

$$\theta = \tan^{-1}\left[\frac{-\omega_b k_z}{2k_x(\omega_c - \omega_0)}\right]. \tag{35}$$

From Equation (32), we see that if $\theta = 90°$, $\omega_c = \omega_0$ and there is no Doppler shift. In this case, it is not possible to measure the velocity of a scatterer with a conventional plane wave. However, with a layered array beam, the velocity can be accurately determined from Equation (33), because there are two peaks in the spectrum of the received pulsed-echo signal that can be used to calculate the bandwidth of the spectrum broadening due to the beam modulation.

Measurement of transverse velocity of moving scatterers such as blood flow was first proposed in [68] with a conventional focused beam. The spectrum due to the transverse beam modulation has a shape of a triangle when the scatterers are near the focus. The spectrum may change with depth, but the minimum and maximum frequencies of the spectrum or the bandwidth are constant for a given velocity. Theoretically, in noise-free environment, the velocity can be determined from the maximum and minimum frequencies. Limited diffraction beams have a large depth of field. Therefore, their spectra have not only constant maximum and minimum frequencies, but also constant shapes over depth. When a Bessel beam is used [31], its spectrum has shoulders at the maximum and minimum frequencies. This helps to increase the accuracy of velocity measurement in a noisy environment, because shoulders can be used to determine the maximum and minimum frequencies.

With layered array beams, the shoulders in the spectrum of a Bessel beam are replaced with peaks. The peaks are easier to locate than the shoulders in a noisy environment, and thus the accuracy of the velocity measurement can be further improved. In addition, layered array beams are easier to implement in practice and can be incorporated into commercial B-scan imagers because their weightings are one dimensional and they can be produced with a linear array [Fig. 5(a)]. Computer simulations have shown that layered array beams are uncoupled between the *x* (lateral) and *y* (elevation) directions. The cosine beam pattern (14) in the lateral direction is the same when the beam is focused in the elevation direction. This means that a lens or a 1.5-dimensional array can be used to focus layered array beams into a thin line in elevation direction [Fig. 5(b)]. By using a pulse, the focused layered array beams can be used to determine the velocity of a parallel line of blood flow within a vessel that is parallel to the linear array. In practice, the position of the vessel can be determined with a conventional B-mode image, and then a layered array beam is used to measure the transverse flow velocity without using a wedge stand. This is useful for velocity measurement of blood flow in vessels that are close and run in parallel to skin. If we are only interested in such vessels (e.g., carotid arteries), high-frequency (e.g., 10-MHz) transducers can be used, since less penetration depth is required. In this case, from Equations (15) and (18), we see that the size of aperture of the transducer can be reduced or the scaling parameter k_x can be increased. A larger k_x increases the bandwidth of the spectrum broadening and thus reduces errors in velocity estimation (33). Further computer simulations and experiments with layered array beams can be done similar to those published in [31]. Better results are expected.

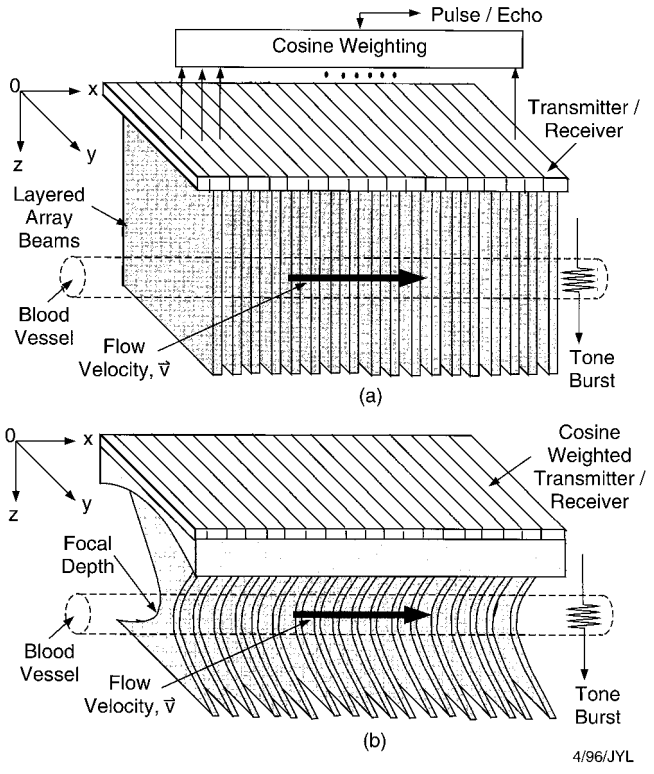

Figure 5. A schematic of a limited diffraction layered array beam [formed by a cosine weighting (14) in the x direction of a linear array] for the measurement of transverse velocity of blood flow. To increase the range or axial resolution, a short tone burst instead of CW wave can be used. In the elevation direction (y direction), the beam can be either unfocused (a) or focused (b). With a focused beam and a short pulse, a thin line within the vessel can be defined, and thus the velocity profile in a vessel can be measured.

V. DISCUSSION

A. Resolution. Lateral resolution of limited diffraction array beams is controlled by the scaling parameters, α, for the Bessel array beams (8), and k_x and k_y for the grid (11) and layered (14) array beams. The larger these constants are, the smaller the beamwidth or the higher the resolution will be. However, these parameters must be smaller than the wave number, k, so that the propagation constants, β (8) and k_z ((11) and (14)), are real. Otherwise, the solutions (8), (11), and (14) will not represent a propagating wave, rather, a decayed vibration along z axis. Because $k = 2\pi/\lambda$, where λ is the wavelength, the maximum lateral resolution is related to the wavelength of beams.

B. Depth of Field. Limited diffraction beams have an infinite depth of field if they are produced with an infinite aperture. When these beams are produced with a finite aperture, they have a large depth of field. It is seen from Equation (15) that the depth of field is determined by the phase velocity c_1, where $c_1 > c$. From Equations (16) to (18), we see that as c_1 increases, the scaling parameters α, k_x, and k_y also increase. This increases the lateral resolution of parallel beams in an array beam [see Eqs. (8), (11), and (14)]. If $c_1 \to \infty$, the lateral resolution will be the highest, but the depth of field will be zero. If $c_1 \to c$, the scaling parameters must be zero and the array beams are actually a truncated plane wave propagating along the z axis [see Eqs. (8), (11), and (14)]. In this case, Equation (15) should be replaced with the Rayleigh distance [35].

C. Sidelobes. Array beams are composed of multiple parallel beams and their side lobes may be as large as the main lobe. However, in real-time volumetric imaging, multiple beams in transmission are required for subsequent parallel receive beam forming. Compared to broad diverging transmit beams [62–65], array beams may increase lateral resolution and have smaller energy in ''side lobes'' (there are gaps between parallel beams). In addition, array beams have the advantage of a large depth of field compared to conventional focused beams. ''Side lobes'' in layered array beams are useful in the measurement of the transverse velocity of blood flow.

D. Volumetric Imaging. Compared to two-dimensional B-mode imaging, volumetric imaging systems are much more complicated. A two-dimensional array transducer of a large number of elements is usually required. The electronics that associate with the array transducer are also very complex because a large number of channels in both transmission and reception is needed. The complexity increases further with the number of parallel beam formers in reception. In addition, there are other complexities, too, such as, huge amount of data coming from the beamforming system need to be processed, stored, and displayed effectively to convey diagnostic information of tissues. However, these problems may be solved in the future as the technologies for two-dimensional arrays and electronics advances.

E. Measurement of Transverse Velocity of Blood Flow. The advantages and limitations of layered array beams for the measurement of the transverse velocity of blood flow are similar to those of Bessel beams given in [31]. However, layered array beams have additional advantages discussed in the Possible Applications section, such as that there are peaks at the maximum and minimum frequencies of the spectrum and they can be implemented with a linear array.

In practice, the aperture of layered array beams is finite. If a layered array beam is truncated in the x direction with a rectangular window,

$$W(x) = \begin{cases} 1; & |x| \le D/2 \\ 0; & \text{Otherwise} \end{cases}, \tag{36}$$

Equation (14) should be modified by multiplying $W(x)$. The spectrum of the modified layered array beams can also be obtained because the multiplication of a function in the spatial domain is equivalent to the convolution in its spatial frequency domain. Apparently, the spectrum peaks in Equations (23) and (27) will be replaced with a sinc function, since the Fourier transform of (36) is a sinc function.

F. Production of Limited Diffraction Array Beams. Weighting functions for limited diffraction array beams [Eqs. (8), (11), and (14)] can be approximated by stepwise functions of

infinite fine steps. This means that a two-dimensional array of an infinite number of elements is needed. In practice, the weighting functions can be approximated with an array of fewer elements. According to the Nyquist sampling theorem, the sampling frequency of an aperture weighting function should be at least twice that of the maximum frequency of the function [76]. In the case of the grid and layered array beams, the highest spatial frequency along the x and y axes is determined by k_x and k_y [see Eqs. (11) and (14)], respectively. Therefore, if the minimum sampling frequency required by the Nyquist theorem is used, the number of elements of transducer arrays for producing the array beams shown in Figure 1(c) and 1(d) can be as few as 145 and 13, respectively, resulting in an alternating phase weighting used previously in the production of Bessel beams [8]. Although the stepwise weightings may have some effects on beams in the near field of individual elements of the transducer arrays, the cosine beam patterns will be recovered in their far field. This is evidenced in [8]. As the sampling frequency is increased from the minimum frequency (number of elements of a transducer array is increased [5]), the influence of stepwise weighting will be diminished quickly because the near-field distance of individual element decreases with the square of the aperture size of the element.

With the analysis above, a two-dimensional array of 145 elements can be used to produce the grid array beam in Figure 1(c). Such array can be used in a real-time volumetric imaging system where 145 parallel pencil beams are transmitted simultaneously and the same number of parallel dynamically focused beams that follow the transmitting beams is formed in reception. To increase the line density within the large aperture (50 mm in diameter), the two-dimensional array can be scanned electronically (similar to the scan in a commercial linear array that requires a larger number of elements) or mechanically in a raster format within a grid area. If 10 A-lines between parallel beams are added, the line density of the cylindrical volume (Fig. 4) will be increased from 145 to about 14,500. The suggested system will have a high image frame rate (30 frame/s) over a distance of 25 cm. Although image frame rate is increased 145 times in this system, the same number of receive beam formers are required, and thus the imaging system will be very complex. Currently, only a system that has 16 parallel beam formers, each of which has 64 channels, has been reported [63].

Because grid array beams have a large depth of field, a real-time volumetric imaging system that has a constant transverse resolution could be constructed by combing the dynamic aperture technique [48] with the dynamically focused reception that maintains a constant f-number everywhere within the imaging volume. A constant resolution may be useful in image restoration because the point spread function of such system will be depth independent.

From Figure 1(d), it is seen that the construction of a transducer for the layered array beam can be simplified if the minimum sampling frequency required by the Nyquist theorem is chosen. To produce the layered array beam in Figure 1(d), 13 elements may be sufficient. This can be done by weighting the output of the array alternatively in phase in both transmit and receive. Because layered array beams (14) are independent of the axis, y, the dimension of the linear array in y should be sufficiently large so that the depth of field (Rayleigh distance) imposed in this direction is equal or larger than that in the x direction (Fig. 5). Because the beam patterns in x and y directions are actually decoupled for layered array beams, a lens or a one-and-a-half dimensional array can be used to focus the beam in the y direction.

G. More Limited Diffraction Beams. Limited diffraction array beams are only examples of new limited diffraction beams. The solution (2) of the wave equation is quite general and its linear combination over free parameters [9,15] may produce more beams that have practical applications.

H. Future Studies. Detailed studies (resolution and contrast) of volumetric imaging systems with limited diffraction array beams can be further studied with computer simulations. Applications of layered array beams for the measurement of transverse velocity of blood flow will be investigated in experiment. Other applications of the new beams will be explored.

VI. CONCLUSION

New limited diffraction beams that are called array beams have been developed. These beams are composed of multiple parallel beams and have an infinite depth of field when produced with an infinite aperture. Even if with a finite aperture, they have a large depth of field. In addition to theory, a synthetic array experiment was performed to produce these beams. The experiment results agree very well with the theory even if the beams are produced with a broadband pulse. The new beams may have potential applications in volumetric imaging and the measurement of transverse velocity of blood flow.

ACKNOWLEDGMENTS

The author thanks Elaine C. Quarve for secretarial assistance. This work was supported in part by Grants CA 54212 and CA 43920 from the National Institutes of Health.

REFERENCES

1. J. Durnin. ''Exact solutions for nondiffracting beams. I. The scalar theory,'' *J. Opt. Soc. Am. A* **4,** 651–654 (1987).
2. J. Durnin, J. J. Miceli, Jr., and J. H. Eberly. ''Diffraction-free beams,'' *Phys. Rev. Lett.* **58,** 1499–1501 (1987).
3. J.-Y. Lu, H.-H. Zou, and J. F. Greenleaf. ''Biomedical ultrasound beam forming,'' *Ultrason. Med. Biol.* **20,** 403–428 (1994).
4. J.-Y. Lu and J. F. Greenleaf, ''Diffraction-limited beams and their applications for ultrasonic imaging and tissue characterization,'' in *New Developments in Ultrasonic Transducers and Transducer Systems.* F. L. Lizzi, Ed., Proceedings SPIE, Vol. 1733, Bellingham, Washington, 1992, pp. 92–119.
5. J.-Y. Lu, T. K. Song, R. R. Kinnick, and J. F. Greenleaf, ''*In vitro* and *in vivo* real-time imaging with ultrasonic limited diffraction beams,'' *IEEE Trans. Med. Imag.* **12,** 819–829 (1993).
6. Jian-yu Lu, M. Fatemi, and J. F. Greenleaf, ''Pulse-echo imaging with X wave,'' in *Acoustic Imaging,* Vol. 22. Piero Tortoli, Ed., Plenum Press, New York, 1996, pp. 191–196.
7. J.-Y. Lu and J. F. Greenleaf. ''Pulse-echo imaging using a nondiffracting beam transducer,'' *Ultrason. Med. Biol.* **17,** 265–281 (1991).
8. J.-Y. Lu and J. F. Greenleaf. ''Ultrasonic nondiffracting transducer for medical imaging,'' *IEEE Trans. Ultrason. Ferroelec. Freq. Control* **37,** 438–447 (1990).
9. J.-Y. Lu. ''Bowtie limited diffraction beams for low-sidelobe and large depth of field imaging,'' *IEEE Trans. Ultrason. Ferroelec. Freq. Control* **42,** 1050–1063 (1995).
10. J.-Y. Lu, H. Zou, and J. F. Greenleaf. ''A new approach to obtain limited diffraction beams,'' *IEEE Trans. Ultrason. Ferroelec. Freq. Control* **42,** 850–853 (1995).
11. J.-Y. Lu, ''Construction of limited diffraction beams with Bessel

bases,'' in *IEEE 1995 Ultrasonics Symposium Proceedings*, 95CH35844, Vol. 2, 1995, pp. 1393–1397.
12. J.-Y. Lu and J. F. Greenleaf, ''Formation and propagation of limited diffraction beams,'' in *Acoustic Imaging*, Vol. 20. Y. Wei and B.-L. Gu, Eds., Plenum Press, New York. 1993, pp. 331–343.
13. H.-H. Zou, J.-Y. Lu, and J. F. Greenleaf. ''Obtaining limited diffraction beams with the wavelet transform,'' in *IEEE 1993 Ultrasonics Symposium Proceedings*, 93CH3301-9, Vol. 2, 1993, pp. 1087–1090.
14. J.-Y. Lu and J. F. Greenleaf. ''Effect on J_0 nondiffracting beam of deleting central elements of J_0 annular array transducer,'' *Ultrason. Imag.* **13,** 203 (1991) (abstr.).
15. J.-Y. Lu and J. F. Greenleaf. ''Nondiffracting X waves—exact solutions to free-space scalar wave equation and their finite aperture realizations,'' *IEEE Trans. Ultrason. Ferroelec. Freq. Control* **39,** 19–31 (1992).
16. J.-Y. Lu and J. F. Greenleaf. ''Experimental verification of nondiffracting X waves,'' *IEEE Trans. Ultrason. Ferroelec. Freq. Control* **39,** 441–446 (1992).
17. T. K. Song, J.-Y. Lu, and J. F. Greenleaf. ''Modified X waves with improved field properties,'' *Ultrason. Imag.* **15,** 36–47 (1993).
18. J.-Y. Lu and J. F. Greenleaf. ''Theory and acoustic experiments of nondiffracting X waves,'' in *IEEE 1991 Ultrasonics Symposium Proceedings*, 91CH3079-1, Vol. 2, 1991, pp. 1155–1159.
19. J.-Y. Lu and J. F. Greenleaf. ''A study of two-dimensional array transducers for limited diffraction beams,'' *IEEE Trans. Ultrason. Ferroelec. Freq. Control* **41,** 724–739 (1994).
20. J.-Y. Lu and J. F. Greenleaf, ''Steering of limited diffraction beams with a two-dimensional array transducer,'' in *IEEE 1992 Ultrasonics Symposium Proceedings*, 92CH3118-7, Vol. 1, 1992, pp. 603–607.
21. J.-Y. Lu and J. F. Greenleaf. ''Sidelobe reduction for limited diffraction pulse-echo systems,'' *IEEE Trans. Ultrason. Ferroelec. Freq. Control* **40,** 735–746 (1993).
22. J.-Y. Lu and J. F. Greenleaf, ''A study of sidelobe reduction for limited diffraction beams,'' in *IEEE 1993 Ultrasonics Symposium Proceedings*, 93CH3301-9, Vol. 2, 1993, pp. 1077–1082.
23. J.-Y. Lu and J. F. Greenleaf. ''Sidelobe reduction of nondiffracting pulse-echo images by deconvolution,'' *Ultrason. Imag.* **14,** 203 (1992) (abstr.).
24. J.-Y. Lu and J. F. Greenleaf, ''Comparison of sidelobes of limited diffraction beams and localized waves,'' in *Acoustic Imaging*, Vol. 21. J. P. Jones, Ed., Plenum Press, New York. 1995, pp. 145–152.
25. J.-Y. Lu and J. F. Greenleaf. ''Experiment of imaging contrast of J_0 Bessel non-diffracting beam transducer,'' *J. Ultrasound Med.* **11(Suppl.),** S43 (1992) (abstr.).
26. J.-Y. Lu and J. F. Greenleaf. ''Simulation of imaging contrast of nondiffracting beam transducer,'' *J. Ultrasound Med.* **10(Suppl.),** S4 (1991) (abstr.).
27. J.-Y. Lu and J. F. Greenleaf, ''Evaluation of a nondiffracting transducer for tissue characterization,'' in *IEEE 1990 Ultrasonics Symposium Proceedings*, 90CH2938-9, Vol. 2, 1990, pp. 795–798.
28. J.-Y. Lu and J. F. Greenleaf. ''Producing deep depth of field and depth-independent resolution in NDE with limited diffraction beams,'' *Ultrason. Imag.* **15,** 134–149 (1993).
29. D. K. Hsu, F. J. Margetan, and D. O. Thompson. ''Bessel beam ultrasonic transducer: fabrication method and experimental results,'' *Appl. Phys. Lett.* **55,** 2066–2068 (1989).
30. J. A. Campbell and S. Soloway. ''Generation of a nondiffracting beam with frequency independent beam width,'' *J. Acoust. Soc. Am.* **88,** 2467–2477 (1990).
31. J.-Y. Lu, X.-L. Xu, H. Zou, and J. F. Greenleaf. ''Application of Bessel beam for Doppler velocity estimation,'' *IEEE Trans. Ultrason. Ferroelec. Freq. Control* **42,** 649–662 (1995).
32. R. W. Ziolkowski. ''Localized transmission of electromagnetic energy,'' *Phys. Rev. A.* **39,** 2005–2033 (1989).
33. J. Ojeda-Castaneda and A. Noyola-Iglesias. ''Nondiffracting wavefields in grin and free-space,'' *Microwave Optic. Technol. Lett.* **3,** 430–433 (1990).
34. G. Indebetow. ''Nondiffracting optical fields: Some remarks on their analysis and synthesis,'' *J. Opt. Soc. Am. A* **6,** 150–152 (1989).
35. G. S. Kino, *Acoustic Waves: Devices, Imaging, and Analog Signal Processing* (Prentice-Hall, Englewood Cliffs, NJ), 1987, Chapters 2 and 3.
36. J. H. McLeod. ''The Axicon: A new type of optical element,'' *J. Opt. Soc. Am.* **44,** 592–597 (1954).
37. C. B. Burckhardt, H. Hoffmann, and P. A. Grandchamp. ''Ultrasound axicon: A device for focusing over a large depth,'' *J. Acoust. Soc. Am.* **54,** 1628–1630 (1973).
38. F. S. Foster, M. S. Patterson, M. Arditi, and J. W. Hunt. ''The conical scanner: A two transducer ultrasound scatter imaging technique,'' *Ultrason. Imag.* **3,** 62–82 (1981).
39. M. Moshfeghi. ''Sidelobe suppression in annular array and axicon imaging systems,'' *J. Acoust. Soc. Am.* **83,** 2202–2209 (1988).
40. M. S. Patterson, F. S. Foster, and D. Lee, ''Sidelobe and speckle reduction for an eight sector conical scanner,'' in *IEEE 1981 Ultrasonics Symposium Proceedings*, 81CH1689-9, Vol. 2, 1981, pp. 632–637.
41. M. S. Patterson and F. S. Foster. ''Acoustic fields of conical radiators,'' *IEEE Transactions on Sonics and Ultrasonics* **SU-29,** 83–92 (1982).
42. J. P. Wild. ''A new method of image formation with annular apertures and application in radio astronomy,'' *Proc. Royal Soc. A* **286,** 499–509 (1965).
43. C. B. Burckhardt, P. A. Grandchamp, and H. Hoffmann, ''Methods for increasing the lateral resolution of B-scan,'' in *Acoustic Holography*, Vol. 5. P. S. Green, Ed., Plenum Press, New York, 1973, pp. 391–413.
44. D. Vilkomerson, ''Acoustic imaging with thin annular apertures,'' in *Acoustic Holography*, Vol. 5. P. S. Green, Ed., Plenum Press, New York, 1973, pp. 283–316.
45. C. B. Burckhardt, P.-A. Grandchamp, and H. Hoffmann. ''Focussing ultrasound over a large depth with an annular transducer—an alternative method,'' *IEEE Transactions on Sonics and Ultrasonics* **SU-22,** pp. 11–15 (1975).
46. A. Macovski and S. J. Norton, ''High-resolution B-scan systems using a circular array,'' in *Acoustic Holography*, Vol. 6. N. Booth, Ed., Plenum Press, New York, 1975, pp. 121–143.
47. R. A. Harris, D. H. Follett, M. Halliwell, and P. N. T. Wells. ''Ultimate limits in ultrasound imaging resolution,'' *Ultrasound Med. Biol.* **17,** 547–558 (1991).
48. D. R. Dietz, S. I. Parks, and M. Linzer. ''Expanding-aperture annular array,'' *Ultrason. Imag.* **1,** 56–75 (1979).
49. J. N. Brittingham. ''Focus wave modes in homogeneous Maxwell's equations: Transverse electric mode,'' *J. Appl. Phys.* **54,** 1179–1189 (1983).
50. R. W. Ziolkowski. ''Exact solutions of the wave equation with complex source locations,'' *J. Math. Phys.* **26,** 861–863 (1985).
51. R. W. Ziolkowski, D. K. Lewis, and B. D. Cook. ''Evidence of localized wave transmission,'' *Phys. Rev. Lett.* **62,** 147–150 (1989).
52. A. M. Shaarawi, I. M. Besieris, and R. W. Ziolkowski. ''Localized energy pulse train launched from an open, semi-infinite, circular waveguide,'' *J. Appl. Phys.* **65,** 805–813 (1989).
53. I. M. Besieris, A. M. Shaarawi, and R. W. Ziolkowski. ''A bidirectional traveling plane wave representation of exact solutions of the scalar wave equation,'' *J. Math. Phys.* **30,** 1254–1269 (1989).
54. E. Heyman, B. Z. Steinberg, and L. B. Felsen. ''Spectral analysis of focus wave modes,'' *J. Opt. Soc. Am. A* **4,** 2081–2091 (1987).
55. J. V. Candy, R. W. Ziolkowski, and D. K. Lewis. ''Transient waves: Reconstruction and processing,'' *J. Acoust. Soc. Am.* **88,** 2248–2258 (1990).
56. J. V. Candy, R. W. Ziolkowski, and D. K. Lewis. ''Transient wave estimation: A multichannel deconvolution application,'' *J. Acoust. Soc. Am.* **88,** 2235–2247 (1990).
57. R. W. Ziolkowski and D. K. Lewis. ''Verification of the localized wave transmission effect,'' *J. Appl. Phys.* **68,** 6083–6086 (1990).

58. R. Donnelly, D. Power, G. Templeman, and A. Whalen. ''Graphic simulation of superluminal acoustic localized wave pulses,'' *IEEE Trans. Ultrason. Ferroelec. Freq. Control* **41,** 7–12 (1994).
59. R. Donnelly and R. W. Ziolkowski. ''Designing localized waves,'' *Proc. Royal Soc. Lond., A* **440,** 541–565 (1993).
60. K. Uehara and H. Kikuchi. ''Generation of near diffraction-free laser beams,'' *Appl. Phys. B* **48,** 125–129 (1989).
61. L. Vicari. ''Truncation of nondiffracting beams,'' *Optics Commun.* **70,** 263–266 (1989).
62. O. T. von Ramm, S. W. Smith, and B. A. Carroll. ''Advanced real-time volumetric ultrasound scanning,'' *J. Ultrasound Med.* **14,** S35 (1995) (abstr.).
63. R. E. Davidsen and S. W. Smith, ''Sparse geometries for two-dimensional array transducers in volumetric imaging,'' in *IEEE 1993 Ultrasonics Symposium Proceedings*, 93CH3301-9, Vol. 2, 1993, pp. 1091–1094.
64. S. W. Smith, H. G. Pavy, Jr., and O. T. von Ramm. ''High-speed ultrasound volumetric imaging system—part I: Transducer design and beam steering,'' *IEEE Trans. Ultrason. Ferroelec. Freq. Control* **38,** 100–108 (1991).
65. O. T. von Ramm, S. W. Smith, and H. G. Pavy, Jr. ''High-speed ultrasound volumetric imaging system—part II: Parallel processing and image display,'' *IEEE Trans. Ultrason. Ferroelec. Freq. Control* **38,** 109–115 (1991).
66. R. L. Goldberg and S. W. Smith, ''Multilayer 2-D array transducers with integrated circuit transmitters and receivers: A feasibility study,'' in *IEEE 1994 Ultrasonics Symposium Proceedings*, 94CH3468-6, Vol. 3, 1994, pp. 1511–1514.
67. C. D. Emery, J. C. Swartz, H. C. Casey, Jr., and S. W. Smith, ''Opto-electronic transmitters for medical ultrasound transducers,'' in *IEEE 1994 Ultrasonics Symposium Proceedings*, 94CH3468-6, Vol. 3, 1994, pp. 1519–1522.
68. V. L. Newhouse, E. S. Furgason, G. F. Johnson, and D. A. Wolf. ''The dependence of ultrasound Doppler bandwidth on beam geometry,'' *IEEE Trans. Sonic. Ultrason.* **SU-27,** 50–59 (1980).
69. J. Ophir. ''Estimation of speed of sound propagation in biological tissues: A beam-tracking method,'' *IEEE Trans. Ultrason. Ferroelec. Freq. Control* **33,** 359–368 (1986).
70. F. John, *Partial Differential Equations* (Springer-Verlag, New York), 1982.
71. P. M. Morse and H. Feshbach, *Methods of Theoretical Physics*, Part I (McGraw-Hill, New York), 1953, Chapters 4–7.
72. P. R. Mesdag, D. de Vries, and A. J. Berkhout, ''An approach to tissue characterization based on wave theory using a new velocity analysis technique,'' in *Acoustic Imaging*, Vol. 12. E. A. Ash and C. R. Hill, Eds., Plenum Press, New York, 1982, pp. 479–491.
73. J.-Y. Lu. ''Producing bowtie limited diffraction beams with synthetic array experiment,'' *IEEE Trans. Ultrason. Ferroelec. Freq. Control* **43,** 893–900 (1996).
74. J.-Y. Lu, ''Construction of limited diffraction beams with Bessel bases,'' in *IEEE 1995 Ultrasonics Symposium Proceedings*, 95CH35844, Vol. 2, 1995, pp. 1393–1397.
75. J.-Y. Lu. ''Designing limited diffraction beams,'' *IEEE Trans. Ultrason. Ferroelec. Freq. Control* (in press).
76. A. V. Oppenheim and R. W. Schafer, *Digital Signal Processing* (Prentice-Hall, Englewood Cliffs, NJ), 1975, Chapter 5.